ACS Medicinal Chemistry Letters

Letter

pubs.acs.org/acsmedchemlett

Discovery of Fluoromethylketone-Based Peptidomimetics as Covalent ATG4B (Autophagin-1) Inhibitors

Zongxing Qiu,[‡] Bernd Kuhn,[§] Johannes Aebi,[§] Xianfeng Lin,[‡] Haiyuan Ding,[‡] Zheng Zhou,[‡] Zhiheng Xu,[‡] Danqing Xu,[‡] Li Han,[‡] Cheng Liu,[‡] Hongxia Qiu,[‡] Yuxia Zhang,[‡] Wolfgang Haap,[§] Claus Riemer,[§] Martin Stahl,[§] Ning Qin,[‡] Hong C. Shen,[‡] and Guozhi Tang*[,‡]

[‡]Roche Pharma Research and Early Development, Therapeutic Modalities, Roche Innovation Center Shanghai, 720 Cailun Road, Shanghai 201203, China

[§]Roche Pharma Research and Early Development, Therapeutic Modalities, Roche Innovation Center Basel, F. Hoffmann-La Roche Ltd., Grenzacherstrasse 124, 4070 Basel, Switzerland

S *Supporting Information*

ABSTRACT: ATG4B or autophagin-1 is a cysteine protease that cleaves ATG8 family proteins. ATG4B plays essential roles in the autophagosome formation and the autophagy pathway. Herein we disclose the design and structural modifications of a series of fluoromethylketone (FMK)-based peptidomimetics as highly potent ATG4B inhibitors. Their structure−activity relationship (SAR) and protease selectivity are also discussed.

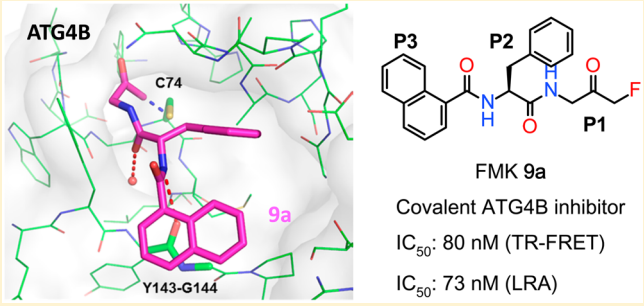

KEYWORDS: *ATG4B, autophagy, covalent inhibitor, fluoromethylketone, peptidomimetics*

Autophagy is an evolutionarily conserved process essential for cell homeostasis and housekeeping by catabolizing aggregated proteins and damaged cellular components.[1] The hallmark of autophagy is the formation of autophagosomes and subsequent fusion with lysosomes to achieve degradation of their contents. Dysregulation of autophagy has been recently described in the pathogenesis of a variety of diseases such as cancer, neurodegenerative and metabolic disorders, and viral infections.[2,3] Modulation of autophagy has become a very active area of preclinical and clinical research, and particularly, there is high interest to identify potent and specific autophagy inhibitors.[4]

ATG4 or autophagins are a class of cytosolic cysteine proteases that cleave ATG8 family proteins, such as light chain 3 (LC3). ATG4 plays essential roles in the formation and maturation of autophagosomes.[5,6] Among all four human ATG4 orthologues, ATG4B is functionally dominant, and it is the sole enzyme reported to efficiently cleave LC3 precursors and to deconjugate lipid from membrane bound LC3-phosphatidylethanolamine (LC3-PE).[7] ATG4B has been considered as a potential therapeutic target in the development of chemosensitizer for the treatment of certain cancer types. Recently, a number of small molecule ATG4B inhibitors such as Z-L-Phe-chloromethylketone and NSC185058 were reported to have modulatory effects on the autophagy process.[8−10] However, because of its high chemical reactivity, the chloromethylketone moiety is usually associated with significant cytotoxicity. NSC185058, however, is only a weak ATG4B inhibitor with an IC_{50} of 51 μM in an assay detecting the cleavage of LC3-GST.[10]

Previously, we reported the identification of Z-FA-FMK (**1**, Figure 1) as a covalent active-site directed ATG4B inhibitor from a TR-FRET based focused library screening.[11] The hit expansion of **1** led to the discovery of Z-FG-FMK (**2**), which was 10-times more potent than **1** with an IC_{50} of 1.2 μM in the biochemical assay.[11] Herein we disclose the structure-guided optimization of **2** toward highly potent fluoromethylketone (FMK)-based ATG4B inhibitors.

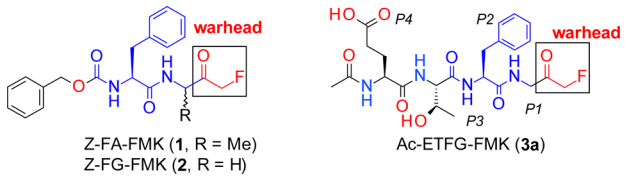

Figure 1. Structures of peptidomimetic ATG4B inhibitors.

As an early step in the autophagosome formation, ATG4B cleaves proLC3 to expose the C-terminal Gly120 for subsequent PE-conjugation and autophagosome membrane insertion.[5] The cocrystal structures of catalytically inert C74S or

Received: May 18, 2016
Accepted: June 25, 2016
Published: June 25, 2016

DOI: 10.1021/acsmedchemlett.6b00208
ACS Med. Chem. Lett. 2016, 7, 802−806

H280A mutant Atg4B in complex with the LC3(1−124) peptide revealed that the substrate induces a conformational change of both the regulatory loop (258−262) and Trp142 resulting in an open protein conformation in which the C-terminal ETFG residues at the processing site of LC3 make several intermolecular contacts with the catalytic pocket of ATG4B.[12] Molecular modeling[13] of compounds **1** and **2** into the open conformation of ATG4B, using the TFG residues of LC3 as template, suggests a potential steric clash of the additional methyl group in **1** with Trp142, which likely explains the inferior anti-ATG4B activity of this molecule (Figure 2).

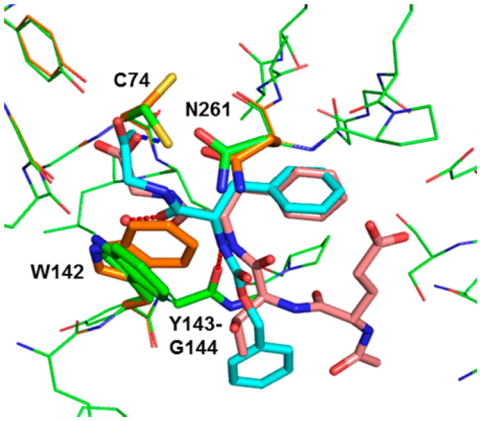

Figure 2. Overlay of the X-ray crystal structure (PDB code: 2Z0D)[12] of the C-terminal LC3 peptide (Glu117-Gly120, salmon) in human ATG4B (orange) with a model of Z-FG-FMK **2** (cyan). Intermolecular hydrogen bonds for **2** are shown as red lines and the covalent interaction with Cys74 is shown in blue. Models were built using the modeling software MOLOC.[13] See also Figure S1 in the Supporting Information for a surface representation of the binding site.

In the predicted binding mode, the FMK warhead makes a covalent bond with the S atom of Cys74 and the planar P1 glycine moiety stacks onto the π-system of the indole ring of Trp142. The benzyl substituent nicely overlaps with the P2 phenylalanine of LC3 and is engaged in dispersion interactions with lipophilic side chains in the S2 pocket as well as stacking interactions with the π-surface of a β-turn. The amide linker connecting P1 and P2 fragments uses its carbonyl oxygen atom to form a hydrogen bond to a buried water molecule. In contrast, in the amide linker between P2 and P3 the NH functionality makes a hydrogen bond with the carbonyl oxygen atom of Tyr143, and the carbonyl group is solvent-exposed. Additionally, the Cbz phenyl ring stacks onto the backbone amide of Tyr143−Gly144.

To investigate the SAR of the C-terminal LC3 peptides, we synthesized and tested a number of FMK-based peptidomimetics including Ac-ETFG-FMK (**3a**, Figure 1) for their ATG4B inhibitory activities. We find that **3a** is about 15 times less active than **2** in the TR-FRET assay and inactive in the cellular based actin-LC3-dNGluc cleavage assay (or luciferase release assay, LRA),[11] probably due to limited cell permeability (Table 1). Moreover, it should be noted that the FMK warhead at the P1 position is important for ATG4B inhibition as peptides like Ac-ETFG (**3b**) and Ac-TFG are inactive in both TR-FRET and LRA assays.

In the first optimization phase we focused on modifications of the warhead and the Phe residue at the P2 position of **2**. Thus, analogues **4a−n** were synthesized (see the Supporting Information) and tested in both TR-FRET and LRA assays. The resulting SAR reveals that formation of a covalent bond to Cys74 is critical for anti-ATG4B activity as direct structural changes of the FMK moiety completely abolish anti-ATG4B activities (examples **4a−b** in Table 1), in agreement with the results of **3a** and **3b**. In addition, we find that many covalent warheads such as pyrazole amide (example **4c**), aldehyde (**4d**), nitrile (**4e−f**), and Michael acceptor-like **4g** are not tolerated either. We hypothesize that this is due to an insufficient fit to the binding site around Cys74 and/or too low reactivity for the formation of a covalent bond.

The chemistry space at the P2 position was explored with a variety of amino acids. For example, (*S*)-α-methyl substitution and amino acids such as (*S*)-phenylglycine, (*S*)-valine, and (*R*)-Phe were incorporated but resulted in a complete loss of anti-ATG4B activity (examples **4h−k**). We find that halogen substituents can be tolerated at the *meta*-position of the phenyl group of **2**. For example, *meta*-Cl analogue **4m** shows an IC_{50} of 1.1 μM in the TR-FRET assay. In contrast, substituents at

Table 1. Inhibition of ATG4B by 1−3 and 4a−n

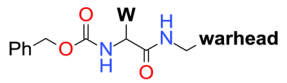

4a-n

ID	W	warhead	IC_{50}-FRET[a]	IC_{50}-LRA[b]
1	Z-FA-FMK		15.0	5.09
2	Z-FG-FMK		1.13	1.47
3a	Ac-ETFG-FMK		17.8	> 100
3b	Ac-ETFG		> 200	> 100
4a	(*S*)-Phe		> 200	> 100
4b	(*S*)-Phe		> 200	> 100
4c	(*S*)-Phe		> 100	ND[c]
4d	(*S*)-Phe		> 100	> 100
4e	(*S*)-Phe		> 200	> 100
4f	(*S*)-Phe		> 200	> 100
4g	(*S*)-Phe		> 100	> 100
4h	(*S*)-α-Methyl Phe		55.1	> 100
4i	(*S*)-Phenylgly		> 200	> 100
4j	(*S*)-Val		> 200	> 100
4k	(*R*)-Phe		> 200	> 100
4l	(*S*)- 		32.1	37.6
4m	(*S*)- 		1.10	1.78
4n	(*S*)- 		4.12	5.68

[a]IC_{50}s [μM] are mean values of TR-FRET experiments in duplicate runs, with variation ±10%. [b]IC_{50}s [μM] are mean values determined by luciferase-release assay (LRA) with Actin-LC3B-dNGLuc construct used in HEK-293T cells. Experiments were run in duplicate with variation ±15%. Compounds were not cytotoxic to HEK-293T cells (CC_{50} > 100 μM) in 24 h treatment. [c]ND, not determined.

DOI: 10.1021/acsmedchemlett.6b00208
ACS Med. Chem. Lett. 2016, 7, 802−806

Scheme 1. Synthesis of FMK-Based ATG4B Inhibitors 8a–k and 9a–h[a]

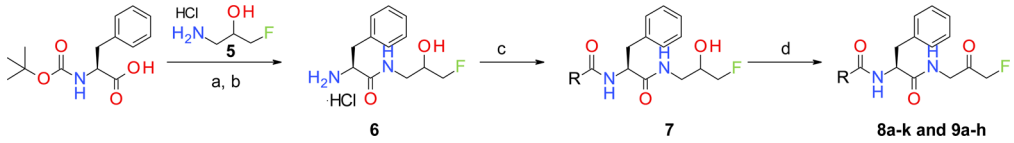

[a]Reagents and conditions: (a) HATU, DIPEA, DMF, rt, 97%; (b) HCl, EtOAc, 30 °C, 30 min, quant.; (c) carboxylic acids, HATU, DMF, rt; (d) DMP, DCM, rt.

ortho- and *para*-positions are clearly detrimental to anti-ATG4B activity (examples including **4l**).

Next, structural explorations were carried out to optimize the terminal *N*-Cbz group. By using the method shown in Scheme 1, (*S*)-*N*-Boc phenylalanine was coupled with 1-amino-3-fluoropropan-2-ol hydrochloride (**5**) in the presence of HATU and DIPEA to give amide product. The *N*-Boc protective group was removed by treating the intermediate with a solution of HCl in EtOAc, and the resulting amine hydrochloride salt **6** was used for further functional transformations. For instance, amine **6** was coupled with selected carboxylic acids to give amides **7**. The FMK group was generated by treating **7** with Dess–Martin periodinane (DMP), and inhibitors **8a–k** were evaluated for their anti-ATG4B activities.

We find that the *N*-Boc analogue **8a** shows comparable activity to **2** with an IC_{50} of 2.0 μM in TR-FRET assay (Table 2). Importantly, the carbamate moiety can be replaced by more

Table 2. Inhibition of ATG4B by 8a–k[a]

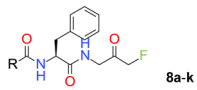

ID	R	IC_{50}-FRET [μM][a]	IC_{50}-LRA [μM][a]
8a		2.03	4.47
8b		9.13	34.3
8c		11.7	13.4
8d		3.76	0.92
8e		1.21	2.57
8f		1.86	4.06
8g		1.01	1.27
8h		0.72	2.99
8i		1.04	1.76
8j		1.00	0.95
8k		3.61	ND

[a]Definitions are the same as those described in Table 1.

rigid and smaller amide moieties, exemplified by benzamide analogue **8e** and cyclopentanecarboxamide **8f**, which demonstrate good anti-ATG4B activities with IC_{50} values of 1.21 and 1.86 μM, respectively. Pyrazine-2-carboxamide analogue **8j** shows promising potency and physicochemical properties, such as a high water solubility of 129 μg/mL in a lyophilized solubility assay (LYSA). Further structural explorations suggest that aryl substituents, especially those at the *meta*-substitution, are well tolerated revealing a rather flat SAR (examples **8g–i**).

Subsequently, bicyclic aromatic groups were used at the P3 position, and the naphthalene-1-carboxamide analogue **9a** showed strong inhibition of ATG4B, with IC_{50} values of 80 and 73 nM in the TR-FRET and cellular-based LRA assays, respectively (Table 3). In comparison, β-substituted analogue

Table 3. Inhibition of ATG4B by 9a–j[a]

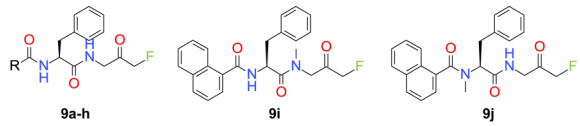

ID	R	IC_{50}-FRET [μM][a]	IC_{50}-LRA [μM][a]
9a		0.080	0.073
9b		1.08	1.19
9c		0.11	0.06
9d		0.057	0.015
9e		0.27	0.53
9f		6.48	12.3
9g		0.19	0.23
9h		4.79	ND
9i	-	0.21	0.13
9j	-	33.1	38.1

[a]Definitions are the same as those described in Table 1.

9b is more than 10 times less active than **9a** probably due to less optimal π-stacking of the β-naphthyl group with the backbone amide. The physicochemical properties of **9a** show moderate solubility (LYSA: 41 μg/mL) and high human and mouse liver microsome clearances of 13.9 and 70 mL min^{-1} kg^{-1}, respectively. Finally, halogen-substitutions and a nitrogen atom walk were carried out on the α-naphthyl group. We find that 5-F substituted analogue **9d** has the best anti-ATG4B activity in our series with an IC_{50} of 15 nM in the cellular LRA assay. We also note that aza-decorations are well tolerated at the 3- and 4-positions but not at the 8-position of the naphthyl group (examples **9e–g**). Both quinoline-4-carboxamide analogue **9e** and cinnoline-4-carboxamide analogue **9g** show strong anti-ATG4B activities and improved solubility compared to **9a** with LYSA values of 188 and 230 μg/mL, respectively. In

DOI: 10.1021/acsmedchemlett.6b00208
ACS Med. Chem. Lett. 2016, 7, 802–806

Table 4. Selectivity of FMK-Based ATG4B Inhibitors[a]

protease family		protease	1	8e	9a
Asp. protease		cathepsin D	>100	>100	>100
Ser. protease		cathepsin G	>100	>100	>100
		tryptase, βII	>100	>100	>100
		neutrophil elastase	>100	>100	>100
Compl. protease		20S proteasome	>100	>100	>100
Cys. proteases	caspase	caspase 2	>100	>100	>100
		caspase 3	43.5	>100	75.1
		caspase 7, 8, 9	>100	>100	>100
	cathepsin	cathepsin B	0.3	0.7	0.2
	others	calpain	0.6	0.6	0.096
metalloprotease		ACE, ECE-1	>100	>100	>100
		MMP1, MMP3, MMP9	>100	>100	>100

[a]IC_{50} apparent [μM] are mean values of protease inhibition from duplicate runs, with variation ±15%. Assays were performed by Genscript according to their standard protocols, see the Supporting Information (www.genscript.com).

addition, they show increased intrinsic metabolic stability compared to **9a**. For example, the human and mouse liver microsome clearances of **9g** are about 9.9 and 39 mL min^{-1} kg^{-1}, respectively.

ATG4B has several solvent-exposed cysteine residues. Nevertheless, ATG4B formed a 1:1 association with FMK analogues after 4 h of coincubation.[11] A subsequent LC−MS/MS study indicated that **9a** formed an irreversible covalent bond with the more reactive thiol group of Cys74 located at the catalytic site of ATG4B. This finding and additional SAR supports our hypothetical binding mode (Figure 2). For example, in our model the P1 amide NH group is not involved in direct ATG4B interactions, while the P2 NH moiety and the backbone carbonyl oxygen of Tyr143 form a hydrogen bond. In line with this binding mode, blocking of both ligand NH groups through *N*-methylation (**9i** and **9j**) is well tolerated at the P1 position (**9i**) but not on the phenylalanine P2 part (**9j**, Table 3). Based on a binding model of **9a** in ATG4B (Figure S2) we postulate that the improved activities of naphthyl analogues of this topology are due to more efficient stacking of the extended bicyclic π-system with the backbone amide group of Tyr143−Gly144.[14] This should be sensitive to the relative orientation of the naphthyl ring to the plane of the adjacent amide linker. This is indeed observed as the preferred orthogonal orientation in the case of α-substitution (**9a**) leads to significantly better ATG4B activity than for β-substitution (**9b**) in which the preferred orientation is close to planar.

FMK analogues **1**, **8e**, and **9a** were selected for target selectivity profiling against a panel of proteases (Table 4). These ATG4B inhibitors have no activity against the aspartic protease, serine proteases, metalloproteases, and the 20S proteasome from our panel. In addition, they show very low inhibition of caspases, which belong to the cysteine protease family. However, the FMK analogues hit a few cysteine proteases such as cathepsin B and calpain with $IC_{50}^{(app)}$ values <1 μM. While the sequence identity is very low between ATG4B and these cysteine proteases, the result can likely be explained by the significant reactivity of the FMK group and the relatively open binding pockets of these proteases. Compound **9a** is slightly more active on ATG4B compared to cathepsin B and calpain. In this study, we did not attempt to further increase the selectivity window through target-based molecular design.

In summary, we discovered a series of highly potent FMK-based covalent ATG4B inhibitors by structural modifications of a focused-library screening hit. Naphthalene-1-carboxamide analogue **9a** and its derivatives inhibit ATG4B with IC_{50} values <100 nM in both a TR-FRET assay and a cell-based luciferase-release assay. The FMK class of ATG4B inhibitors are inactive in a panel of different proteases involving cysteine proteases like caspase 2, 3, 7, 8, and 9. However, they inhibit cathepsin B and calpain with submicromolar IC_{50} values. The SAR of the current FMK series and biostructure differences between ATG4B and other cysteine-proteases support further structural modifications to increase target selectivity. An LC-MS/MS study demonstrated that analogue **9a** forms an irreversible and selective covalent bond with Cys74 and thus inactivates ATG4B proteolytic activity. A binding mode of our series in ATG4B was constructed by molecular modeling revealing key protein−ligand interactions. Efforts including modulation of warhead reactivity and bioisostere replacements of the P1 amide group as well as autophagy modulation effects by analogues of **9a** will be the subject of future publications.

EXPERIMENTAL METHODS

Molecular Docking of FMK Analogues. Model building was performed with the cocrystal structure of human ATG4B with LC3 (1−120) as template (PDB code: 2Z0D)[12] using the following procedure: (1) in silico mutation of the TFG residues of LC3 into Z-FA(G)-FMK; (2) rebuilding of A280H using the structure 2Z0E[12] to reproduce the human sequence; (3) removal of the fluorine atom of Z-FA(G)-FMK and formation of a covalent bond between the sulfur atom of Cys74 and the reactive methylene unit of FMK. Here, the second, alternate conformation of the side chain of Cys74 in the crystal structure 2Z0D was used as this is closer to the FMK group. (4) Minimization of the ligand within the mostly rigid protein allowing for relaxation of only few selected residues (e.g., Tyr54, Cys71, Trp142, Asn261) in close contact to the small molecule.

TR-FRET Assay. Five microliters of serial-diluted test compounds (1% DMSO) in assay buffer was added into 5 μL of purified ATG4B (final 0.1 nM) in 384-well plate, and the solution was incubated at rt for 30 min. Then, 5 μL of His-GATE-16-GST (final 20 nM) was added into the wells, and the solution was incubated at rt for another 30 min. Five microliters of detection solution (final 2 nM of Eu-anti-His and 20 nM of Ulight-anti-GST) was added, and the resulting mixture was incubated at rt for 40 min. The fluorescence signal was measured with Envision4 (Ex, 340 nm; Em, 665/615 nm) and data was analyzed by Genedata Screener (Genedata AG).

Luciferase Release Assay (LRA). A similar procedure has been reported before.[15] Basically, HEK-293T cells (human embryonic kidney cells, ATCC, CRL-11268) were seeded in 6-well plate with a density of 70% confluence. One microgram of enzyme expression plasmid and 2 μg of substrate expression plasmid were cotransfected

DOI: 10.1021/acsmedchemlett.6b00208
ACS Med. Chem. Lett. 2016, 7, 802−806

using 9 μL of X-tremeGENE HP DNA Transfection Reagent (Roche diagnostics cat#06366236001). Three combinations (pCNDA3.1 vector and dNGluc, HTRA4 and Actin-dNGluc, and ATG4B and Actin-LC3-dNGluc) were used in the transfections. After 24 h, the transfected cells were trypsinized, suspended, and transferred to 96-well plates (Corning, can#3599), serial-diluted compounds in assay buffer were added into the platesm and the mixture was incubated for 24 h. Fifty microliters of cell supernatant was transferred to a 96-well white plate (Corning, Cat#3917), and luciferase signal was detected by using BioLux Gaussia luciferase assay kit (NEW ENGLAND BioLabs, Cat#E3300L) and measured with Envision4.

■ ASSOCIATED CONTENT

Supporting Information

The Supporting Information is available free of charge on the ACS Publications website at DOI: 10.1021/acsmedchemlett.6b00208.

Synthetic procedures and analytical data for compounds **2**−**5**, **8a**−**k**, and **9a**−**j**; predicted binding models of Z-FG-FMK (**2**) and **9a**; general assay protocols for evaluation of protease selectivity (PDF)

■ AUTHOR INFORMATION

Corresponding Author

*Phone: +86 21 28946723. E-mail: gordon.tang@roche.com.

Notes

The authors declare no competing financial interest.

■ ACKNOWLEDGMENTS

We are grateful to Qinshan Gao, Yujuan Gao, and Jin Ge for purification of final compounds.

■ ABBREVIATIONS

ATG4B, autophagy-related gene 4B; Cbz, carbobenzyloxy or benzyloxy carbamate; DMP, Dess−Martin periodinane; LC3, light chain 3; LRA, luciferase release assay; LYSA, lyophilized solubility assay; PE, phosphatidylethanolamine; TR-FRET, time-resolved fluorescence energy transfer

■ REFERENCES

(1) Kobayashi, S. Choose delicately and reuse adequately: the newly revealed process of autophagy. *Biol. Pharm. Bull.* **2015**, *38*, 1098−103.
(2) Rubinsztein, D. C.; Codogno, P.; Levine, B. Autophagy modulation as a potential therapeutic target for diverse diseases. *Nat. Rev. Drug Discovery* **2012**, *11*, 709−30.
(3) Kumar, A.; Singh, U. K.; Chaudhary, A. Targeting autophagy to overcome drug resistance in cancer therapy. *Future Med. Chem.* **2015**, *7*, 1535−42.
(4) Cheng, Y.; Ren, X.; Hait, W. N.; Yang, J. M. Therapeutic targeting of autophagy in disease: biology and pharmacology. *Pharmacol. Rev.* **2013**, *65*, 1162−97.
(5) Zhang, L.; Li, J.; Ouyang, L.; Liu, B.; Cheng, Y. Unraveling the roles of Atg4 proteases from autophagy modulation to targeted cancer therapy. *Cancer Lett.* **2016**, *373*, 19−26.
(6) Yang, Z.; Wilkie-Grantham, R. P.; Yanagi, T.; Shu, C. W.; Matsuzawa, S.; Reed, J. C. ATG4B (Autophagin-1) phosphorylation modulates autophagy. *J. Biol. Chem.* **2015**, *290*, 26549−61.
(7) Tran, E.; Chow, A.; Goda, T.; Wong, A.; Blakely, K.; Rocha, M.; Taeb, S.; Hoang, V. C.; Liu, S. K.; Emmenegger, U. Context-dependent role of ATG4B as target for autophagy inhibition in prostate cancer therapy. *Biochem. Biophys. Res. Commun.* **2013**, *441*, 726−31.
(8) Shu, C. W.; Madiraju, C.; Zhai, D.; Welsh, K.; Diaz, P.; Sergienko, E.; Sano, R.; Reed, J. C. High-throughput fluorescence assay for small-molecule inhibitors of autophagins/Atg4. *J. Biomol. Screening* **2011**, *16*, 174−82.
(9) Nguyen, T. G.; Honson, N. S.; Arns, S.; Davis, T. L.; Dhe-Paganon, S.; Kovacic, S.; Kumar, N. S.; Pfeifer, T. A.; Young, R. N. Development of fluorescent substrates and assays for the key autophagy-related cysteine protease enzyme, ATG4B. *Assay Drug Dev. Technol.* **2014**, *12*, 176−89.
(10) Akin, D.; Wang, S. K.; Habibzadegah-Tari, P.; Law, B.; Ostrov, D.; Li, M.; Yin, X. M.; Kim, J. S.; Horenstein, N.; Dunn, W. A., Jr. A novel ATG4B antagonist inhibits autophagy and has a negative impact on osteosarcoma tumors. *Autophagy* **2014**, *10*, 2021−35.
(11) Xu, D.; Xu, Z.; Han, L.; Liu, C.; Zhou, Z.; Qiu, Z.; Lin, X.; Tang, G.; Shen, H.; Aebi, J.; Riemer, C.; Kuhn, B.; Stahl, M.; Mark, D.; Qin, N.; Ding, H. Identification of new ATG4B inhibitors based on a novel high-throughput screening platform. *J. Biomol. Screening* **2016**, DOI: 10.1177/1087057116639202.
(12) Satoo, K.; Noda, N. N.; Kumeta, H.; Fujioka, Y.; Mizushima, N.; Ohsumi, Y.; Inagaki, F. The structure of Atg4B-LC3 complex reveals the mechanism of LC3 processing and delipidation during autophagy. *EMBO J.* **2009**, *28*, 1341−50.
(13) Gerber, P.; Müller, K. MAB, a generally applicable molecular force field for structure modelling in medicinal chemistry. *J. Comput.-Aided Mol. Des.* **1995**, *9*, 251−268.
(14) Harder, M.; Kuhn, B.; Diederich, F. Efficient stacking on protein amide fragments. *ChemMedChem* **2013**, *8*, 397−404.
(15) Ketteler, R.; Seed, B. Quantitation of autophagy by luciferase release assay. *Autophagy* **2008**, *4*, 801−806.

DOI: 10.1021/acsmedchemlett.6b00208
ACS Med. Chem. Lett. 2016, 7, 802−806